


# A model based investigation of evaporative cooling for polymer electrolyte fuel cells – System level analysis

**Journal Article****Author(s):**

Striednig, Michael; [Schmidt, Thomas](#) ; Buchi, Felix N.

**Publication date:**

2022-09-15

**Permanent link:**

<https://doi.org/10.3929/ethz-b-000557732>

**Rights / license:**

[Creative Commons Attribution-NonCommercial-NoDerivatives 4.0 International](#)

**Originally published in:**

Journal of Power Sources 542, <https://doi.org/10.1016/j.jpowsour.2022.231720>



# A model based investigation of evaporative cooling for polymer electrolyte fuel cells – System level analysis

Michael Striednig<sup>a</sup>, Thomas J. Schmidt<sup>a,b</sup>, Felix N. Büchi<sup>a,\*</sup>

<sup>a</sup> Electrochemistry Laboratory, Paul Scherrer Institut, Forschungsstrasse 111, CH-5232, Villigen PSI, Switzerland

<sup>b</sup> Laboratory of Physical Chemistry, ETH Zürich, Vladimir-Prelog Weg 1-5/10, CH-8093, Zürich, Switzerland

## HIGHLIGHTS

- Interactions between evaporatively cooled PEFC stack and auxiliaries are analyzed.
- Optimized operating conditions for evaporatively cooled systems are quantified.
- A closed water loop is possible over a wide range of operating conditions.
- An efficiency map for evaporative cooling is proposed.
- The condenser is identified as the one critical component for evaporative cooling.

## ARTICLE INFO

### Keywords:

Polymer electrolyte fuel cell system  
PEFC  
Evaporative cooling  
Modelling  
Zero-dimensional  
Balance of plant

## ABSTRACT

Evaporative cooling is a promising concept to reduce the fuel cell system volume and mass significantly. This paper investigates the interactions between the fuel cell stack and the balance of plant in an evaporatively cooled polymer electrolyte fuel cell system (PEFCS). For this, a zero-dimensional PEFCS model, comprising the fuel cell stack, air compressor, charge air cooler, humidifier, hydrogen recirculation blower, condensing radiator and water separator has been developed and analyzed. Two evaporative cooling system architectures are compared to conventional, liquid cooling. Optimal operating conditions are determined by a numerical optimization of the net system power output. Main results show that evaporative cooling works on the system level over a wide range of operating conditions. The optimum system power and highest efficiencies are achieved at high temperatures (80–90 °C), low pressure (125–150 kPa) and a corresponding cathode stoichiometry between 1.5 and 3, allowing for a closed water loop at the same time. The air compressor shows an increased power demand, compared to conventional cooling and the exhaust gas condenser is identified as the one critical component for evaporative cooling. Its performance is key to an efficient operation and closed water loop at all ambient conditions.

## 1. Introduction

Polymer electrolyte fuel cells (PEFC) are an auspicious alternative to internal combustion engines (ICE) and lithium-ion batteries for passenger cars [1–3] but especially for heavy-duty transport applications [4,5]. They allow an emission free conversion of hydrogen, show high system efficiencies (>60%) [3], high power densities (640 W/L) [6] and good dynamic behavior as well as excellent freeze start capabilities [7]. Further, the direct use of hydrogen allows fast refueling [8], high mileage [9] and allows a temporal decoupling of electricity production and vehicle refueling, which reduces the concurrent power demand for refueling substantially. However, PEFC costs, durability as well as power

density have to be further improved to become a viable alternative [10–12].

Heat rejection is challenging for conventional fuel cell electric vehicles (FCEV). U.S. Department of Energy (DOE) estimates the maximum heat rejection of FCEV at 1.45 kW/K, which significantly limits the continuous power output of fuel cell systems. Furthermore, the cooling system is directly and indirectly responsible for a significant share of fuel cell stack and system volume. On the one hand, a complex multi-layer bipolar plate design is required in order to guide the liquid coolant through each cell of the stack [13]. Hence, bipolar plates account for 75% of stack volume [14]. On the other hand, conventional cooling requires high operating temperatures to facilitate the heat rejection.

\* Corresponding author.

E-mail address: [felix.buechi@psi.ch](mailto:felix.buechi@psi.ch) (F.N. Büchi).

<https://doi.org/10.1016/j.jpowsour.2022.231720>

Received 13 March 2022; Received in revised form 15 May 2022; Accepted 1 June 2022

Available online 17 June 2022

0378-7753/© 2022 Paul Scherrer Institut. Published by Elsevier B.V. This is an open access article under the CC BY-NC-ND license (<http://creativecommons.org/licenses/by-nc-nd/4.0/>).

Therefore, an external humidifier is often required to ensure proper humidification and thus ionic conductivity of the polymer electrolyte membrane [15].

Evaporative cooling is a promising concept to overcome the heat rejection limitation. At the same time, it enables a significant reduction of stack and system volume as well as cost by simplifying the design of bipolar plates and eliminating the need for external humidification. Evaporative cooling approaches have been presented in several articles and patents [16–28]. All share the fact that the system complexity is increased compared to conventional cooling.

The PSI evaporative cooling concept [29] is based on a specially designed gas diffusion layer (GDL) with patterned wettability [30]. Liquid water is supplied to the cell, where it is subsequently wicked into the hydrophilic part of the GDL and distributed across the active area. When the water evaporates, it cools the cell and concurrently humidifies the membrane, which yields a higher ionic conductivity thereof. This allows higher operating temperatures without the need for external humidification and simplifying the design of bipolar plates, thus showing the potential of reduced system volume, mass, complexity and cost by up to 30%.

However, the interactions between the fuel cell stack and balance of plant (BoP) are complex. Hence, numerical models can improve the understanding of the relevant interdependencies. Numerous articles have investigated the evaporation of liquid water as well as the two-phase transport in gas diffusion layers [31–39], setting the ground for several numerical and experimental studies that have analyzed evaporative cooling in differential single cells [29,40] and on stack level [16, 17].

Evaporative cooling has been investigated on the system level by Schultze and Horn [41], who developed a control oriented simulation model. They considered the heat exchanger as well as water separator, a cooling water tank, water pumps and the fuel cell stack. Simulations were in good agreement with experimental data. However, the specific requirements of the auxiliaries in an evaporatively cooled fuel cell system have not been analyzed.

Hwang and Kim [17] investigated liquid water injection into the cathode gas supply experimentally. In their study, they focused on the cathode humidification and cooling of the stack by water atomization. Balance of plant components have not been considered in further detail. They investigated the water spray formed with an external-mixing air-assist atomizer and identified the optimal water pressure. Choi et al. [16] performed a parametric analysis of evaporative cooling and humidification by liquid water injection in a 5 cell stack. They investigated the influence of water temperature, pressure as well as relative humidity of the air stream on the evaporation rate and stack performance.

Fly and Thring [42] developed a fuel cell vehicle model for evaporative cooling. They investigated the thermal and water balance. The impact of operating pressure on the waste heat was studied. They have shown that at increased pressure, an increased operating temperature is required, which reduces the required frontal area of the radiator. In further studies, they have focused on the temperature regulation of the fuel cell stack [43] as well as on a detailed analysis of the exhaust gas condenser [44]. They have proven that the frontal area of a condensing radiator can be reduced by 30%, compared to a conventional heat exchanger.

In our previous study [45], we have investigated the potentials and limits of evaporative cooling numerically on the stack level. A zero-dimensional model has been developed, incorporating mass and energy balances as well as electrochemical performance and evaporation. We have shown that evaporative cooling is feasible on the stack level over a wide range of operating conditions and proposed an operating window, which is slightly shifted towards higher temperatures (80–95 °C), lower pressures (100–200 kPa) and higher cathode stoichiometries (>1.5) compared to conventional fuel cells. Additionally, we have listed the challenges of the evaporative cooling approach.

Despite the fact that evaporative cooling has been the focal point of many studies, the interactions between the fuel cell stack and balance of plant have not been analyzed in detail in literature yet. Furthermore, the water balance of an evaporatively cooled fuel cell system has not been investigated systematically so far.

Therefore, this study aims at analyzing the effect of the air compressor and the anode recirculation as well as the exhaust gas condenser on the fuel cell stack operation. A detailed parameter study and numerical optimization is performed to identify optimal operating conditions in order to achieve highest system efficiencies within the boundaries of a closed water loop (i.e. conditions that allow to condense the amount of water from the exhaust, which is required by the stack for evaporative cooling). For this, a zero-dimensional fuel cell system model has been developed where this study focuses on the BoP interactions. Two different system architectures for evaporative cooling are investigated and the net system power is compared to a conventionally cooled fuel cell system.

## 2. Numerical methods

In order to analyze the interactions within an evaporatively cooled fuel cell system and to determine suitable operating conditions, a fuel cell system model has been developed. It allows fast parameter studies and the application of numerical optimization methods. A model-based approach has been chosen since experimental studies are expensive, time consuming and require a highly integrated test infrastructure [46, 47]. Furthermore, a semi-empirical, zero-dimensional approach is justified by the complex interactions between different scales of the hydrophilic/hydrophobic pattern (500 µm hydrophilic lines with 1000 µm spacing) and the channel length of about 160 mm. To correctly capture the coupled through-plane and down-the-channel effects of evaporative cooling with a physical model, a multi-dimensional, two-phase approach would be required, which in turn would lead to significant computational costs which would make the application of the presented optimization schemes impossible.

### 2.1. Overview and assumptions

Three different fuel cell system architectures are investigated in this work, evaporative cooling at the cathode, at the anode and conventional cooling (see Fig. 1). All three models contain the fuel cell stack, air compressor (AC), charge air cooler (CAC), hydrogen recirculation blower (HRB), as well as anode and cathode water separators (AWS, CWS). The conventional model (Fig. 1a) additionally comprises a humidifier (HUM), whereas the evaporative cooling models include a condensing radiator (COND) that is either positioned at the cathode exhaust (Fig. 1b) or in the anode recirculation loop (Fig. 1c). The cathode backpressure valve, hydrogen injector as well as purge and drain valves are not modeled. Instead, an ideal control of the anode and cathode stack outlet pressure and a constant nitrogen concentration in the anode recirculation loop (ideal purge behavior) are assumed. The power consumption of the coolant pump is neglected in this study as is the DC/DC converter and a potential turbine/expander. The target of the model is to obtain the stack performance and water demand, the compressor and HRB power consumption as well as the condensation rates from the exhaust gas at different operating conditions to define optimal operating strategies with maximized net system power at thermal steady state and closed water loop. Further, the impact of condenser outlet temperature on the evaporative cooling performance is investigated.

The developed model is zero-dimensional in nature and simulates the thermal steady state of the stack. In the context of this work, zero-dimension means that each component is modeled zero-dimensionally (i.e. no spatial extent is considered) and the output of one component serves as an input to the subsequent one. Output and input consider species molar flowrates, as well as total pressure and temperature. Heat

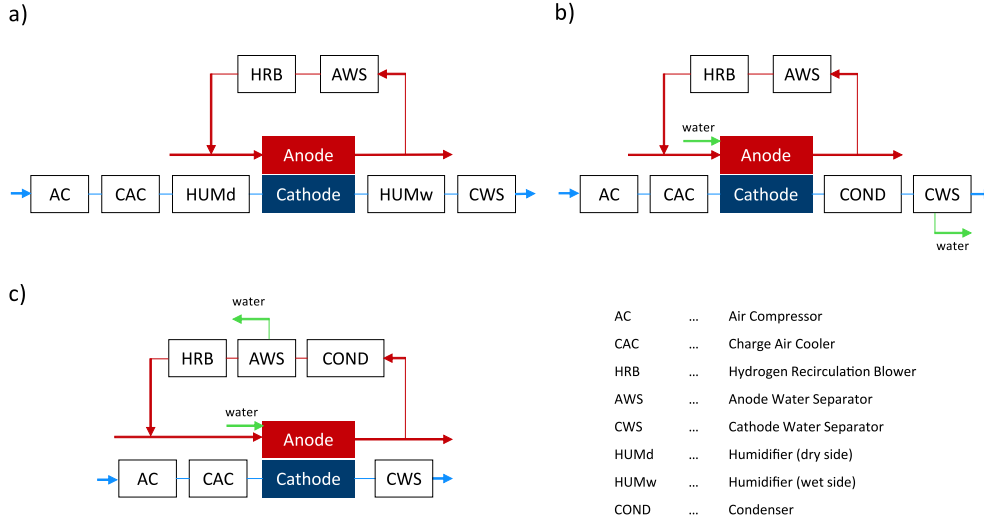


Fig. 1. Investigated fuel cell system architectures. a) conventional liquid cooling, b) cathode evaporation concept, c) anode evaporation concept.

and pressure losses of connecting pipes are neglected since they are assumed to be short and properly insulated. Thermal steady state, on the other hand, indicates the condition at which the entire waste heat of the stack is removed by evaporative cooling and thus the stack temperature remains constant. However, variables can still change in time. The presented equations yield a system of ordinary differential equations (ODE) in time, which has been solved with Simulink® (Version 9.0, R2017b, © The MathWorks, Inc.). The integrated *ODE45* solver [48] (i.e. Dormand Prince Method [49]) has been used with variable step size [45].

The following assumptions and simplifications have been made:

- i. Perfect gas behavior (i.e. constant specific heat capacities) and mixtures of perfect gases are assumed for the BoP models (see supplementary information for more details).
- ii. Fully saturated gases (RH = 100%) at anode and cathode outlet respectively condenser inlet are assumed (see Lal et al. [35]).
- iii. Heat and pressure losses of pipes connecting components are neglected.
- iv. Ideal evaporation: all produced heat evaporates water and evaporation is only limited by saturation of the gas in the flow channels of the stack.
- v. Ideal water supply: the same amount of water that can evaporate is supplied.
- vi. Water is only considered in vapor phase (except for the water supply and condenser outlet).
- vii. Nitrogen crossover is neglected ( $N_2$  volume fraction equals zero in the anode recirculation loop).
- viii. Anode purge losses are neglected.

Assumptions applied to the fuel cell stack model are summarized in our previous work [45].

The different sub-models of the three investigated system architectures are discussed in more detail in the following chapters. Further, the

applied optimization strategy is described.

## 2.2. Fuel cell stack model

In the fuel cell stack model, the steady-state mass balance (1) and energy balance (2), as well as the electrochemical performance (3) are taken into account. In order to enhance the readability, only the governing equations are presented here. A more detailed description of the stack model is published in our previous work [45].

$$\sum \dot{n}_i + \dot{n}_{i,s} = 0 \quad (1)$$

where  $\dot{n}_i$  denotes the molar flow rates of the species  $i$  across the system boundaries and  $\dot{n}_{i,s}$  is the respective sink or source term inside the control volume.

$$\dot{Q}_{\text{surf}} + P_{\text{el}} + \sum \dot{m}_i (h_i + e_{a,i}) = \frac{dU}{dt} = 0 \quad (2)$$

The transfer of heat  $\dot{Q}_{\text{surf}}$  and electrical power  $P_{\text{el}}$  as well as enthalpy and external energy of mass flow  $\dot{m}_i (h_i + e_{a,i})$  across the system boundary changes the internal energy  $dU$  of the system. For steady-state conditions, the change in internal energy equals zero.

To calculate the actual cell voltage  $E_{\text{cell}}$ , the various overpotentials (kinetic losses of the oxygen reduction reaction  $\eta_{\text{ORR}}$ , the ohmic losses due the ionic resistance of the membrane  $j \cdot R_{\text{mem}}$  and the contact resistances  $j \cdot R_{\text{cont}}$ , the proton transport losses in the cathode catalyst layer  $j \cdot R_{\text{H}^+}$  and the mass transport overpotential  $\eta_{\text{tx},\text{O}_2}$ ) are subtracted from the reversible cell voltage  $E_{\text{rev}}$ . The protonic resistance of the anode catalyst layer and the kinetic overpotential of the hydrogen oxidation reaction (HOR) are neglected [50].

$$E_{\text{cell}} = E_{\text{rev}} - \eta_{\text{ORR}} - j \cdot R_{\text{mem}} - j \cdot R_{\text{cont}} - j \cdot R_{\text{H}^+} - \eta_{\text{tx},\text{O}_2} \quad (3)$$

The evaporation rate  $\dot{n}_{\text{H}_2\text{O}}^{\text{ev,max}}$  can be calculated with the assumption of fully saturated exhaust gas streams from the mass balance as follows:

$$\dot{n}_{\text{H}_2\text{O}}^{\text{ev,max}} = \dot{n}_{\text{H}_2\text{O}}^{\text{liq,in}} = \frac{j \cdot A_{\text{act}}}{2 \cdot F} k \left[ \frac{\frac{p_{\text{sat}}^{\text{out}}}{p_{\text{tot}}^{\text{out}}} \left( \lambda_a \left( \nu_{\text{N}_2,\text{dry}}^{\text{a,in}} / \nu_{\text{H}_2,\text{dry}}^{\text{a,in}} + 1 \right) + \frac{\lambda_c}{2} \left( \nu_{\text{N}_2,\text{dry}}^{\text{c,in}} / \nu_{\text{O}_2,\text{dry}}^{\text{c,in}} + 1 \right) - \frac{3}{2} \right)}{\left( 1 - \frac{p_{\text{sat}}^{\text{out}}}{p_{\text{tot}}^{\text{out}}} \right)} - 1 \right] \quad (4)$$

with system pressure  $p_{\text{tot}}$ , anode and cathode stoichiometric ratios  $\lambda_a$ ,  $\lambda_c$ , dry gas composition of cathode and anode supply  $\nu_{\text{N}_2, \text{dry}}^{\text{c, in}}$ ,  $\nu_{\text{O}_2, \text{dry}}^{\text{c, in}}$ ,  $\nu_{\text{N}_2, \text{dry}}^{\text{a, in}}$ ,  $\nu_{\text{H}_2, \text{dry}}^{\text{a, in}}$  as well as current density  $j$ , active area per cell  $A_{\text{act}}$ , number of cells  $k$ , saturation pressure  $p_{\text{sat}}^{\text{out}}$  (as a function of temperature  $T$ ) and Faraday constant  $F$  [45].

With the molar enthalpy of evaporation of water  $\Delta H_{\text{m, H}_2\text{O}}^{\text{ev}}$ , the corresponding cooling power  $P_{\text{cool}}^{\text{ev, max}}$  can be calculated as follows:

$$P_{\text{cool}}^{\text{ev, max}} = \dot{n}_{\text{H}_2\text{O}}^{\text{ev, max}} \cdot \Delta H_{\text{m, H}_2\text{O}}^{\text{ev}} \quad (5)$$

From the energy balance, the following steady-state condition can then be derived:

$$jA_{\text{act}}k \left( \frac{-\Delta H_{\text{m}}^{\text{r}}}{2F} - E_{\text{cell}} \right) = k_{\text{fc}} A_s (T_c - T_{\text{amb}}) + \dot{n}_{\text{H}_2\text{O}}^{\text{ev, max}} \cdot \Delta H_{\text{m, H}_2\text{O}}^{\text{ev}} \quad (6)$$

where  $\Delta H_{\text{m}}^{\text{r}}$  is the molar enthalpy of reaction,  $k_{\text{fc}}$  is the heat transfer coefficient to the environment,  $A_s$  is the surface area of the stack and  $T_{\text{amb}}$  is the ambient temperature. The steady-state condition allows to determine suitable combinations of operating conditions at which the entire waste heat is removed by evaporative cooling. See Ref. [45] for more details.

In addition to the stack model presented in Ref. [45], the pressure drop of cathode and anode has been implemented. Section 2.3 presents the two different pressure drop models used in this work. For the stack, a linear pressured drop correlation is assumed due to the laminar flow in the gas channels, which contribute to the majority of the stack pressure loss.

### 2.3. Pressure drop correlations

Since the exact geometries of the components are unknown, an empirical approach, considering pressure drop fitting factors ( $\zeta$ ) has been chosen. The parametrization of  $\zeta$  for the different components is provided in the supplementary information.

A linear correlation with volumetric flow (see equation (7)) is assumed for the components, where laminar flow is predominant (i.e. the fuel cell stack and the humidifier).

$$\Delta p_{\text{lam}} = \zeta \mu \dot{V} \quad (7)$$

with pressure drop  $\Delta p$ , viscosity  $\mu$ , volumetric flowrate  $\dot{V}$  and fitting factor  $\zeta$ .

For the charge air cooler, anode and cathode water separator, as well as for the condenser, turbulent flow is assumed to be predominant, therefore a quadratic pressure loss correlation is considered:

$$\Delta p_{\text{turb}} = \zeta \rho \dot{V}^2 \quad (8)$$

with gas density  $\rho$ , which has been calculated as a function of pressure, temperature and the gas composition. For the viscosity  $\mu$ , the pressure dependence has been neglected.

### 2.4. Air compressor and hydrogen recirculation blower model

The compression of air or hydrogen respectively from pressure  $p_1$  to  $p_2$  is modeled as an isentropic compression [51]. Subsequently, the losses due to real compression as well as mechanical (compressor) and electrical losses (electric motor and inverter) are accounted for by the isentropic efficiency  $\eta_s$  and the combined mechanical and electrical efficiency  $\eta_{\text{m, el}}$ . Perfect gas behavior is assumed (i.e. constant specific heat capacity, averaged between  $T_1$  and  $T_2$ )

$$P_{\text{eff}} = \frac{\dot{m} \cdot (h_2 - h_1)}{\eta_{\text{m, el}}} = \frac{P_s}{\eta_s \eta_{\text{m, el}}} = \frac{\dot{m} (h_{2, s} - h_1)}{\eta_s \eta_{\text{m, el}}} \approx \frac{\dot{m} \bar{c}_p (T_{2, s} - T_1)}{\eta_s \eta_{\text{m, el}}} \quad (9)$$

where  $P_{\text{eff}}$  is the compressor/HRB power demand,  $\dot{m}$  is the mass flow of the gas mixture,  $h_2$  is the specific enthalpy of the compressed gas,  $h_1$  is the specific enthalpy at inlet condition and  $h_{2, s}$  is the specific enthalpy after isentropic compression. The enthalpy change from inlet to outlet is approximated for perfect gases as  $\bar{c}_p \cdot (T_{2, s} - T_1)$ . Where  $T_1$  is the inlet temperature,  $T_{2, s}$  is the isentropic outlet temperature and  $\bar{c}_p$  the averaged specific heat capacity at constant pressure. More information on the approximation of  $\bar{c}_p$  is provided in the supplementary information.

Finally, the temperature  $T_{2, s}$  can be calculated for an isentropic compression as follows:

$$\frac{T_{2, s}}{T_1} = \left( \frac{p_2}{p_1} \right)^{\frac{\kappa-1}{\kappa}} \quad (10)$$

where  $\kappa$  is the ratio of the specific heat capacities ( $c_p/c_v$ ).

The inlet pressure  $p_1$  and outlet pressure  $p_2$  are depending on the stack outlet pressure set point as well as on the sum of the component pressure drops, depending on the system architecture (Fig. 1). For the air compressor, the inlet pressure  $p_1$  is approximated with the ambient pressure (i.e. neglected pressure loss of the air filter).

### 2.5. Condenser model

The condenser model allows the calculation of the water condensation rate as a function of the condenser outlet temperature ( $T_{\text{out}}$ ). A reasonable gap to the environment has to be considered. It is assumed that water only exists in vapor state at the condenser inlet (i.e. no liquid water is present). Further, the gas at the condenser inlet is fully saturated due to the high water vapor production rates by evaporative cooling. The condenser is modeled ideal in the sense that the set outlet temperature is always reached (i.e. it is assumed that the area of the condenser is sufficiently large at all simulation conditions).

The condensation rate  $\dot{n}_{\text{cond}}$  can be calculated as the difference between the water vapor flow rate of the saturated gas at the inlet  $\dot{n}_{\text{H}_2\text{O}}^{\text{g, in}}$ , at temperature  $T_{\text{in}}$  and at the condenser outlet  $\dot{n}_{\text{H}_2\text{O}}^{\text{g, out}}$ , at temperature  $T_{\text{out}}$ .

$$\dot{n}_{\text{cond}} = \dot{n}_{\text{H}_2\text{O}}^{\text{g, in}} - \dot{n}_{\text{H}_2\text{O}}^{\text{g, out}} = \left( \frac{\nu_{\text{H}_2\text{O}}^{\text{in}}}{1 - \nu_{\text{H}_2\text{O}}^{\text{in}}} - \frac{\nu_{\text{H}_2\text{O}}^{\text{out}}}{1 - \nu_{\text{H}_2\text{O}}^{\text{out}}} \right) \cdot \dot{n}_{\text{dry}} \quad (11)$$

where  $\nu_{\text{H}_2\text{O}}^{\text{in}}$  and  $\nu_{\text{H}_2\text{O}}^{\text{out}}$  are the mole fractions of water vapor at condenser inlet and outlet respectively and  $\dot{n}_{\text{dry}}$  is the molar flowrate of the dry gas (hydrogen at the anode and oxygen and nitrogen at the cathode). For mixtures of perfect gases, this can be written as a function of saturation pressure and total pressure as follows:

$$\dot{n}_{\text{cond}} = \left( \frac{P_{\text{sat}}^{\text{in}}}{p_{\text{tot}}^{\text{in}} - P_{\text{sat}}^{\text{in}}} - \frac{P_{\text{sat}}^{\text{out}}}{p_{\text{tot}}^{\text{out}} - P_{\text{sat}}^{\text{out}}} \right) \cdot \dot{n}_{\text{dry}} \quad (12)$$

where  $p_{\text{sat}}$  is the water saturation pressure at temperature  $T_{\text{in}}$  and  $T_{\text{out}}$ , respectively, which has been determined according to Antoine's equation. See supplementary information for details. The flow rate of dry gas  $\dot{n}_{\text{dry}}$ , as well as the gas temperature  $T_{\text{in}}$  are provided by the stack sub model.

The pressure drop of the condenser is assumed quadratic according to eq. (8). Furthermore, it is assumed, that the flow of the gas phase is mainly contributing to the pressure drop, therefore the flowrate of liquid water has been neglected. To accommodate for the changes throughout the condenser, the average temperature and gas flow rate between inlet and outlet has been considered for the pressure drop calculation.

### 2.6. Charge air cooler, water separator and humidifier models

For the charge air cooler, the anode and cathode water separator as well as for the humidifier, only the pressure drop is modeled. For the water separators and the charge air cooler, a quadratic pressure loss

correlation is considered, whereas the pressure drop in the humidifier is modeled linear. Besides that, the mentioned components are idealized. That means, the outlet conditions are set points, which are achieved under all operating conditions. Thus, the charge air cooler cools the heated air stream down to the set stack temperature, the humidifier provides the set cathode inlet RH (and transfers the same amount of water from the cathode exhaust) and the water separator removes all liquid water from the exhaust stream.

## 2.7. Optimization of net system power

In order to determine the optimal operating strategy, a numerical optimization has been conducted, maximizing the net power output of the fuel cell system. It has been approximated as the difference between stack power ( $P_{\text{stack}}$ ), compressor power ( $P_{\text{AC}}$ ) and HRB power consumption ( $P_{\text{HRB}}$ ). The parasitic power consumptions of other BoP have been neglected since they are small compared to the compressor and HRB power.

$$P_{\text{net}} = P_{\text{stack}} - P_{\text{AC}} - P_{\text{HRB}} \quad (13)$$

Newton's method was used to vary pressure and the secant method was applied to find the corresponding cathode stoichiometry to achieve the maximum net system power, so that a complete removal of the waste heat by evaporative cooling is given at any time. Furthermore, the cathode outlet pressure of the optimized scenario must not fall below ambient pressure. The optimization has been carried out at current densities between 0 and 3.0 A/cm<sup>2</sup> and temperatures between 60 and 90 °C. Further details are provided in the supplementary information.

$$P_{\text{net}} = f(p, \lambda_c) \dots \max$$

$$s.t. \frac{dT_s}{dt} = 0 \quad (\text{all heat is removed by evaporative cooling}) \quad (14)$$

$$j = \text{const.}, T = \text{const.}; p_{\text{out}} > 100 \text{ kPa}, \lambda_c > 1$$

## 3. Results and discussion

In the following sections, the simulation results of the analyzed components as well as their implications on the system behavior are discussed. The basis for this analysis is a system with a stack of about 120 kW gross power (i.e. 450 cells with an active area of 300 cm<sup>2</sup> each).

In order to achieve thermal steady state, the evaporatively cooled fuel cell stack has to be operated at a defined combination of operating parameters (see eqs. (4) and (6)). Since the evaporation rate and thus the evaporative cooling performance decreases with increased pressure, the

**Table 1**  
Simulated test cases and corresponding conditions.

	test case 1: Conventional Cooling	test case 2: Cathode Evaporation	test case 3: Anode Evaporation
Cathode stoichiometry	2	Optimized	2
Anode recirculation rate	1.5 (100% RH)	1.5 (100% RH)	Optimized <sup>a</sup>
Anode nitrogen content	0 vol%	0 vol%	0 vol%
Stack outlet pressure	200 kPa	Optimized	Optimized
HRB isentropic efficiency		50%	
HRB mech., el. efficiency		80%	
Air compressor isentropic efficiency		75%	
Air compressor mech., el. efficiency		80%	

<sup>a</sup> RH depending on condenser outlet temperature.

cathode or anode stoichiometry has to be adapted as a compensation measure, to maintain a constant temperature (at constant load). See Ref. [45] for further details.

Therefore, two different evaporative cooling approaches are discussed in this work. Either the evaporation at the cathode is increased by adjusting the cathode stoichiometry (test case 2, system architecture Fig. 1b) or the evaporation at the anode is optimized by adjusting the anode recirculation rate (test case 3, system architecture Fig. 1c). The performance of both evaporative cooling approaches is compared to a conventional system (test case 1, system architecture Fig. 1a). Table 1 gives an overview of the three test cases and the corresponding simulation conditions. The electrochemical parameters used for the stack model are presented in Ref. [45].

### 3.1. Compressor and HRB power consumption

First, the power consumption of the air compressor and the hydrogen recirculation blower in an evaporatively cooled system (test cases 2 and 3) are discussed and compared to a conventional system with liquid cooling (test case 1).

#### 3.1.1. Cathode evaporation concept

At first, the cathode evaporation concept is discussed. Fig. 2a shows the dependence between operating pressure and cathode stoichiometry in order to maintain a constant temperature at a current density of 1 A/

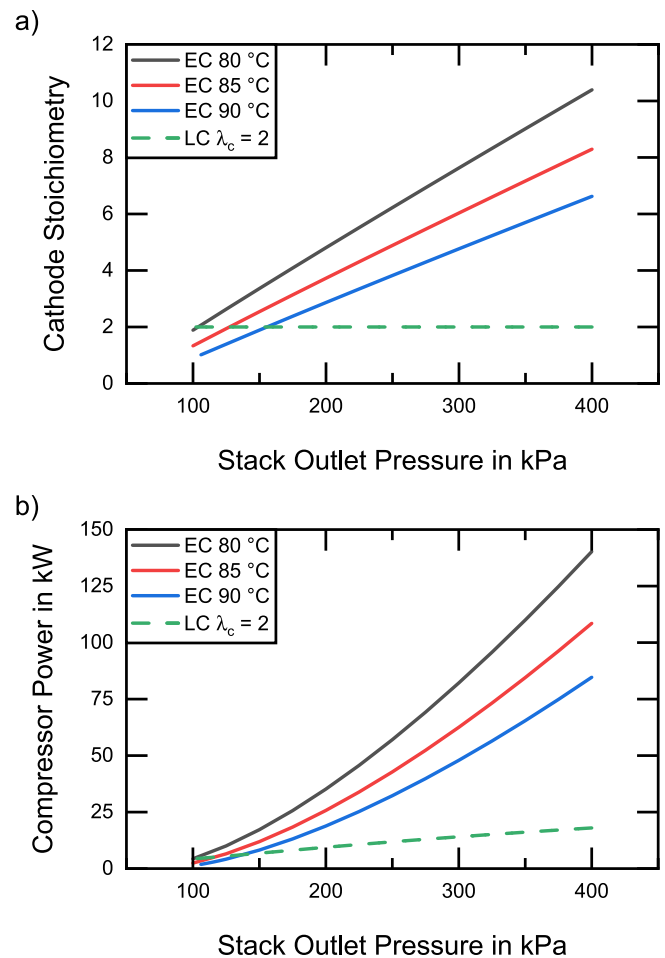


**Fig. 2.** a) Required cathode stoichiometry and b) compressor power consumption as a function of stack outlet pressure and operating temperature to achieve thermal steady state at 1 A/cm<sup>2</sup>; evaporative cooling (EC, solid lines) compared to conventional liquid cooling (LC, dashed line) at a constant cathode stoichiometry of 2.



cm<sup>2</sup>.

It can be seen that the cathode stoichiometry increases almost linearly with pressure over the investigated range to ensure a thermal steady state. Higher temperatures require a lower stoichiometry at the same pressure to achieve a certain evaporation rate (eq. (4)). Furthermore, the gradient in Fig. 2a decreases with increasing temperature, since the cathode stoichiometry affects the evaporation rate and thus cooling performance stronger at higher temperatures and pressures (i.e. a stronger relative sensitivity of the evaporative cooling power towards cathode stoichiometry is observed, see Fig. 4 in Ref. [45]).

Moreover, the required steady-state cathode stoichiometry at low pressure and high temperature drops below 1.5, which is considered a minimum to operate the stack robustly. Operating the evaporatively cooled stack at higher stoichiometry than the steady-state stoichiometry would yield an increased evaporation and cooling power, which would decrease the stack temperature. This effect can theoretically be mitigated by limiting the water supply to the stack, however, this might lead to an unstable operation.

The observed dependence between stoichiometry and operating pressure, affects the power consumption of a compressor providing such characteristics. See eqs. (9) and (10).

Fig. 2b shows the compressor power consumption in the evaporatively cooled system at different steady-state temperatures (solid lines) compared to a conventional system at a constant cathode stoichiometry of 2 (dashed line). It can be seen, that for evaporative cooling, the power demand increases over-proportionally with pressure due to the simultaneous increase in stoichiometry. Furthermore, Fig. 2b shows that the compressor power demand can even offset the stack power, especially at lower operating temperatures and high pressures, where a very high stoichiometry is required to provide sufficient cooling power. Therefore, only the pressure range below 200 kPa and an increased operating temperature above 80 °C are considered relevant for evaporative cooling.

### 3.1.2. Anode evaporation concept

In the anode evaporation concept, the situation is similar. The recirculated hydrogen has to be dried by condensing the water vapor to enable evaporation at the anode. Furthermore, the recirculation rate has to be increased significantly to achieve sufficient evaporation rates. Since a substantial amount of water vapor is removed with the cathode exhaust gas, achieving a closed loop in the anode evaporation concept is more challenging. Fig. 3a shows the required anode stoichiometry as a function of stack outlet pressure to provide a thermal steady state.

First, it can be seen that the required anode stoichiometry increases almost linearly with pressure and it decreases with temperature. This is in line with the results presented for the cathode evaporation concept above, however, the required stoichiometric ratios are significantly higher for the anode evaporation concept, because no nitrogen is present according to our assumptions and the recirculated hydrogen is not completely dried by the condenser.

However, due to the fact that only the pressure drop of the anode recirculation loop has to be overcome, the power consumption of the hydrogen recirculation blower (HRB) is smaller compared to the air compressor. Fig. 3b shows that the HRB power increases over-proportionally with pressure. This can be explained by the over-proportionally increased pressure drop of the anode recirculation loop at increased pressure and increased stoichiometry. In comparison to the low power consumption of the HRB in a conventional system (dashed line), a significantly higher power is observed for evaporative cooling. Also in the anode evaporation concept, lower pressures and increased temperatures are favorable from an HRB power consumption perspective, even though the effects are less pronounced compared to the cathode evaporation concept.

Note: a condenser outlet temperature of 25 °C (best case scenario) is assumed for the calculations provided here. A more detailed discussion on the interactions between condenser outlet temperature and required

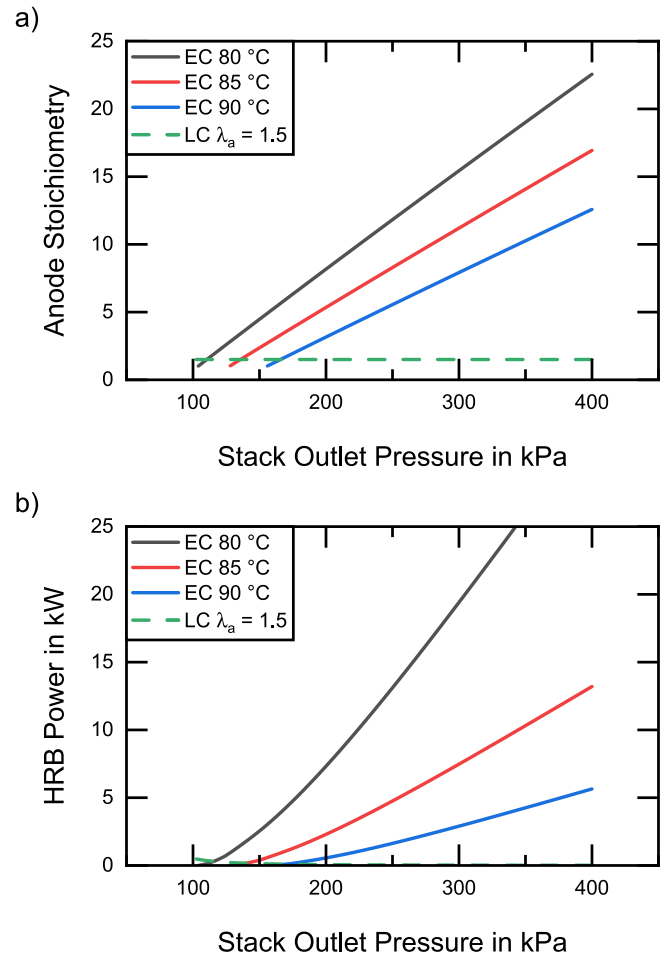


Fig. 3. a) Steady-state anode stoichiometry and b) hydrogen recirculation blower (HRB) power consumption as a function of stack outlet pressure and operating temperature. Evaporative cooling (EC, solid lines) is compared to conventional liquid cooling (LC, dashed lines) at a current density of 1 A/cm<sup>2</sup> and a condenser outlet temperature of 25 °C.

anode stoichiometry as well as system power is presented below in section 3.3.2. Furthermore, the impact of the nitrogen concentration in the anode recirculation loop is not taken into account. The results presented here, are considered the best case scenario. Additional N<sub>2</sub> in the anode recirculation loop requires an increased HRB power consumption to achieve the same evaporation rate, since the pressure drop of the anode recirculation loop increases due to the increased density and viscosity of the mixture (eq. (7) and (8)). The increased massflow in eq. (9), however, is mostly offset by the decrease in the specific heat capacity (the molar heat capacities at constant pressure ( $c_{mp}$ ) of hydrogen and nitrogen only differ insignificantly at 80 °C [52]).

## 3.2. Net system power

Next, the impact of the operating conditions on the net system power is discussed. Operating temperature, pressure and stoichiometry affect the evaporation rate, BoP power consumption as well as the stack performance significantly.

### 3.2.1. Cathode evaporation concept

Fig. 4a illustrates the simulated stack power as a function of operating pressure and temperature. The cathode stoichiometry is chosen such that the thermal steady state is achieved. It can be seen that the impact of temperature is strongest at low pressure whereas it is negligible at high operating pressure. The higher temperatures result in a

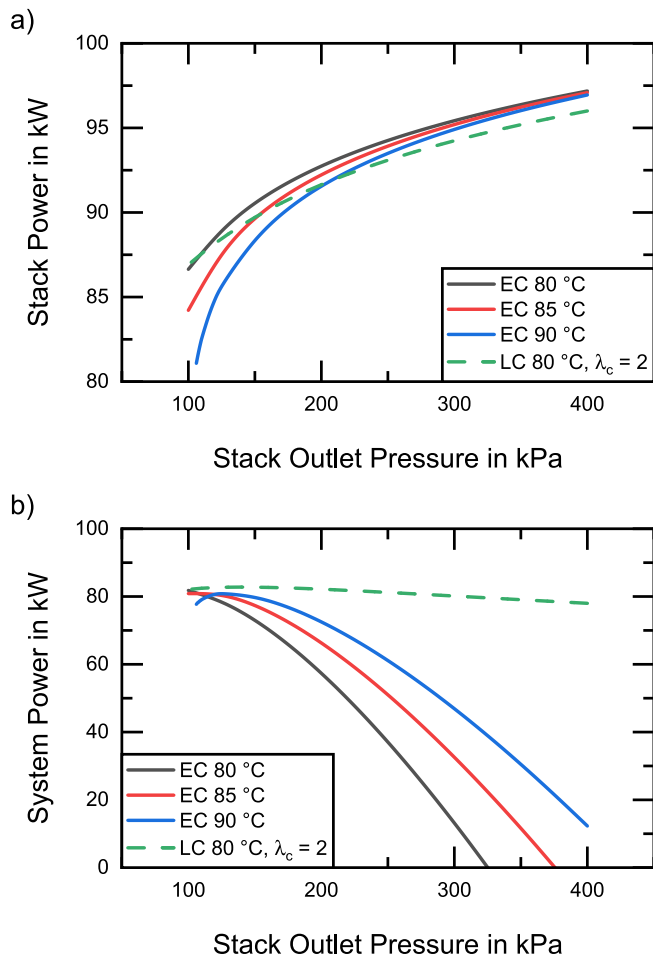


**Fig. 4.** a) stack power and b) system power as a function of stack outlet pressure and operating temperature for the cathode evaporation concept. Evaporative cooling (EC, solid lines) is compared to conventional operation with liquid cooling (LC, dashed lines).

higher water partial pressure which reduces the oxygen partial pressure and thus the stack performance. This effect is more pronounced at lower pressure and additionally enhanced by the lower steady-state stoichiometry at higher temperatures. Furthermore, the decrease in Nernst potential with increasing temperature is more pronounced than the decrease in ORR overpotential, see Ref. [45].

Fig. 4b shows the net system power of an evaporatively cooled system at different temperatures (solid lines) compared to a conventional system (dashed line) at  $1 \text{ A/cm}^2$ . Since the increase in compressor power consumption is more pronounced with higher operating pressure (see Fig. 2b) than the increase in stack power (see Fig. 4a), the net system power shows a maximum at low operating pressure. However, at very low pressure, this is compensated by a significant drop in stack power. Therefore, the maximum is more or less pronounced, depending on the operating temperature. It can be seen, that the optimal system power at  $1 \text{ A/cm}^2$  is rather independent of the operating temperature, however, it is achieved at different system pressures and corresponding stoichiometric ratios. Based on these results, the optimal operating pressure for the cathode evaporation concept is found between 125 and 150 kPa, depending on the operating temperature. Furthermore, the maximal system power is only slightly lower in comparison to conventional operation (green dashed line).

### 3.2.2. Anode evaporation concept

In the anode evaporation concept, the stack power does not show such a strong dependence on temperature than in the cathode

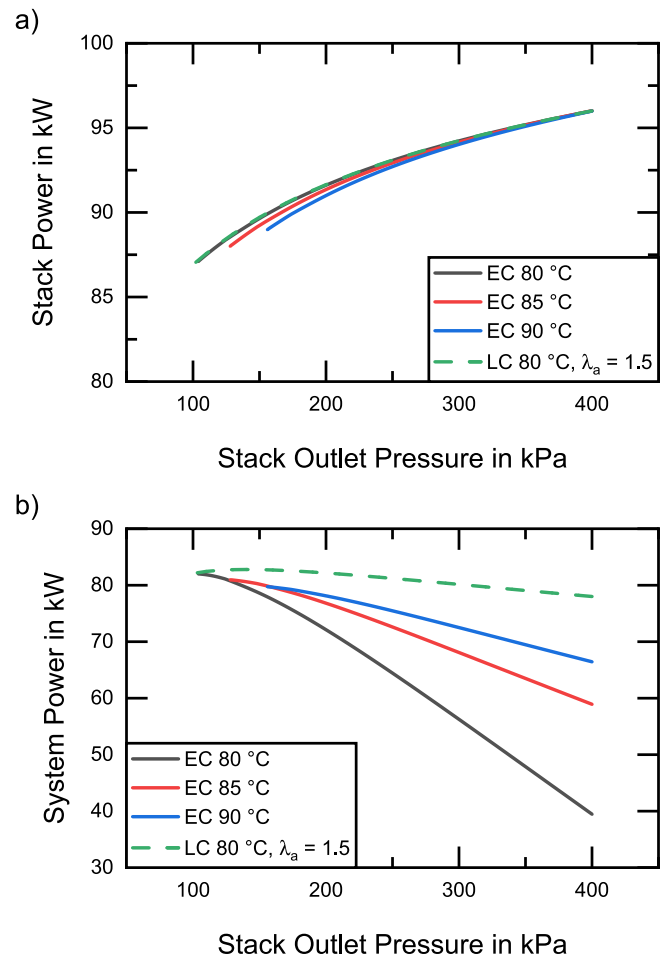


**Fig. 5.** a) stack power and b) system power as a function of stack outlet pressure and operating temperature for the anode evaporation concept. Evaporative cooling (EC, solid lines) is compared to conventional operation with liquid cooling (LC, dashed lines).

evaporation concept. We attribute this to the fact that in this concept the anode stoichiometry is varied whereas the cathode stoichiometry is held constant at 2. Since the anode stoichiometry shows less impact on the cell voltage, the stack power in Fig. 5a is mainly depending on the stack pressure. The little impact of the temperature at lower pressure is explained by the decreased oxygen partial pressure and the decreased Nernst potential.

The power consumption of the HRB in the anode evaporation concept is lower compared to the air compressor in the cathode evaporation concept. Therefore, the system power at high pressure is higher in the anode evaporation concept (see Fig. 5b). However, at low pressure this effect is less pronounced and thus the peak system power is comparable in both concepts and only slightly lower than in the conventional system.

### 3.3. Exhaust gas condenser

The exhaust gas condenser is a critical component for the evaporatively cooled system. However, its impact is different in the two investigated concepts.

#### 3.3.1. Role of the condenser in the cathode evaporation concept

In the cathode evaporation concept, the condenser outlet temperature does not directly affect the system power nor the required evaporation rate to achieve a thermal steady state, since there is no recirculation on the cathode side and thus dry air is supplied to the stack,



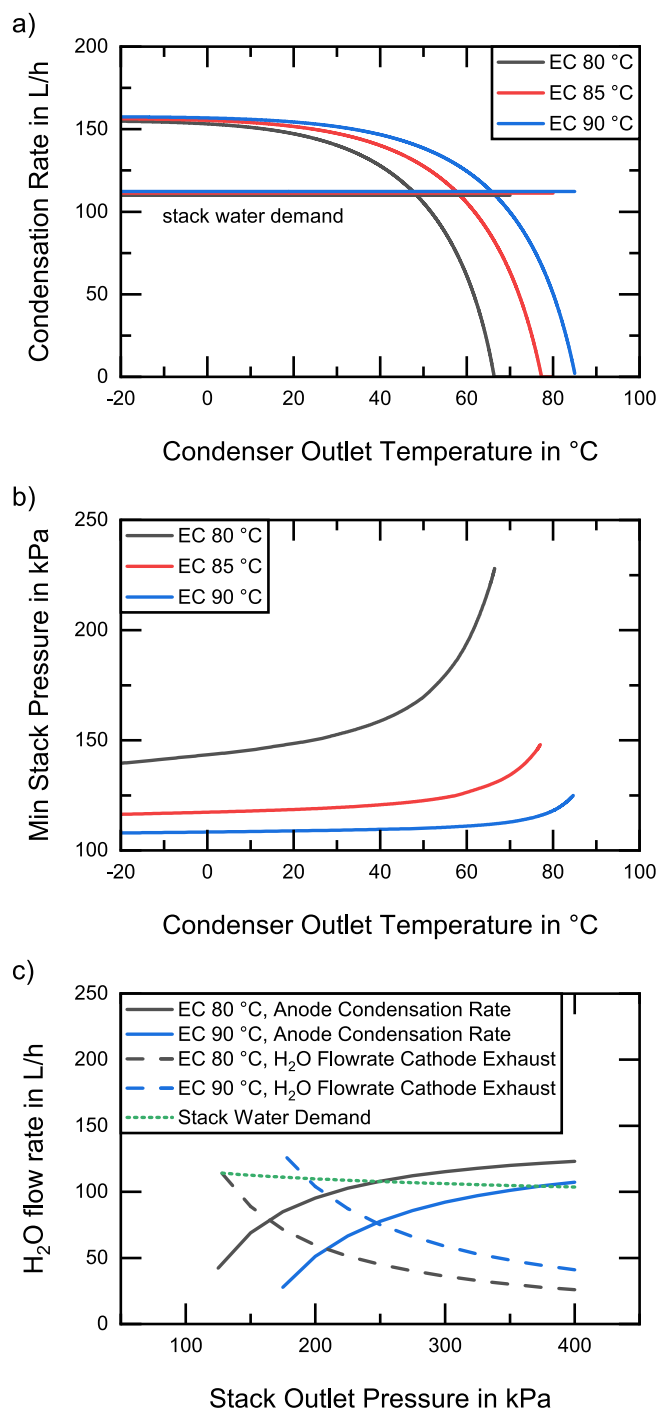


**Fig. 6.** a) Condensation rate for cathode (solid) and corresponding stack water demand (dashed) as a function of condenser outlet temperature at different operating temperature. b) minimal stack outlet pressure as a function of condenser outlet temperature and operating temperature. Both at optimized operating conditions (pressure and cathode stoichiometry) to achieve max. power output at a current density of 1 A/cm<sup>2</sup>. c) anode condensation rate (solid), cathode exhaust water flow rate (dashed) and stack water demand (dotted) as a function of stack outlet pressure at 1 A/cm<sup>2</sup> and a cathode stoichiometry of 2.

independent of the condenser. Furthermore, it is observed that the operating conditions of the stack do not impact the water demand (i.e. evaporation rate), nor the amount of water that is available in the exhaust gas significantly (assuming a thermal steady state and constant load). Therefore, average values are presented for the cathode

condensation rates.

Calculated condensation rates are mainly affected by the condenser outlet temperature and the operating temperature. Fig. 6a shows the condensation rates for the cathode evaporation concept at three different operating temperatures (solid lines). It can be seen that condensation starts below the actual operating temperature and increases with decreasing condenser outlet temperature. Fully saturated gas streams are assumed at the condenser inlet, however, due to the pressure drop of the condenser, the condensation starts below the actual operating temperature. At very low temperatures, the condensation rate plateaus since essentially all water vapor that is contained in the exhaust gas is condensed. All operating temperatures show a similar peak condensation rate, since the pressure and stoichiometry are optimized to remove all waste heat. The slight difference is explained by slightly changed fuel cell performance and thus waste heat production at the different operating conditions.

The condensation rates are generally higher at higher operating temperatures since there is a larger difference to the condenser outlet temperature, which yields a higher difference in water partial pressure. This effect is stronger at higher temperatures since the saturation pressure shows an exponential behavior with temperature. E.g. cooling the 90 °C fully saturated exhaust gas by 20 °C yields higher condensation rates than cooling the 80 °C exhaust gas by 20 °C.

Therefore, the required minimal condenser outlet temperature to enable a closed water loop (i.e. to condense the amount of water from the exhaust gas that is required by the stack to remove the entire waste heat by evaporative cooling) can be determined by intersecting the condensation rates with the stack water demand in Fig. 6a. It can be seen that an operating temperature of 80 °C would require a condenser outlet temperature slightly below 50 °C to condense the water demand from the cathode exhaust gas. This might be challenging to achieve at all environmental conditions. At 90 °C, however, the required condenser outlet temperature is slightly below 70 °C.

Further, Fig. 6a shows that the water demand of the stack can be completely satisfied by condensing water only from the cathode exhaust. A sufficient amount of water vapor is available at all steady-state operating conditions. Since no evaporation takes place at the anode in this scenario (saturated hydrogen is recirculated), an increased water demand and thus evaporation rate (e.g. at higher loads) is solely reflected by an increased water vapor flowrate at the cathode exhaust.

However, the condenser outlet temperature also has an impact on the amount of uncondensed water vapor. This, in turn, affects the pressure drop of the condenser, since it is assumed that the gas phase mainly contributes to the pressure drop. Therefore, the condenser outlet temperature indirectly limits the minimal stack outlet pressure (i.e. ambient pressure + condenser pressure drop). Fig. 6b shows the impact of the condenser outlet temperature on the minimal stack outlet pressure. It can be seen, that the impact is lowest for the highest operating temperature since the lowest stoichiometry and thus flowrate is required.

The above-mentioned effects clearly indicate the benefit of higher operating temperatures for the evaporative cooling concept. Furthermore, the condenser is identified as the one critical component for the cathode evaporation concept, since it determines the minimal operating pressure and thus the net system power and efficiency.

### 3.3.2. Role of the condenser in the anode evaporation concept

In the anode evaporation concept, the role of the condenser is different. Since humid exhaust gas is recirculated, the condenser outlet temperature determines the relative humidity at the anode inlet and thus the evaporation rate in the stack. To achieve a thermal steady state, a higher RH at the stack inlet needs to be compensated by a higher anode recirculation rate. Thus, the condenser outlet temperature indirectly affects the HRB power consumption (due to the increased recirculation rate) and therefore the net fuel cell system power. The provided calculations of the net system power in section 3.1.2 assume a condenser

outlet temperature of 25 °C and therefore a best-case scenario. The condensation rate at thermal steady state, however, is independent of the condenser outlet temperature, since a higher outlet temperature would be compensated by a higher stoichiometry to achieve the required evaporation and thus condensation rate. An explanatory figure is presented in the supplementary information.

The evaporation does not exclusively occur at the anode in this concept. Therefore, the amount of water recoverable in the anode exhaust also depends on the evaporation at the cathode (since both are considered when determining the steady-state evaporation rate) and thus on the operating conditions (i.e. temperature, pressure and cathode stoichiometry). Fig. 6c shows the impact of the aforementioned parameters on the water vapor flow rate at cathode exhaust and thus on the achievable condensation rate at the anode. In order to provide a sufficiently high condensation rate at the anode (solid lines), the evaporation at the cathode has to be reduced. The minimal operating pressure at different operating temperatures can be found by intersecting the condensation rates (solid lines) with the stack water demand (green dotted line). Considering these minimal operating pressure (about 250 kPa at 80 °C and 360 kPa at 90 °C), the peak of the corresponding system power (Fig. 5b) can by far not be reached with the anode only evaporation concept. Even at a decreased cathode stoichiometry of 1.5, the net system power is lower as compared to the cathode evaporation concept.

Furthermore, the anode evaporation concept is more complex from an engineering perspective, since water has to be continuously separated from the hydrogen rich recirculation gas without risking safety or additional hydrogen losses while draining liquid water. Additionally, more powerful hydrogen recirculation blowers are required which would contribute to increased system volume and mass. Further, this is not in line with current trends towards a passive anode recirculation (i.e. ejector solution). Therefore, the anode evaporation concept is not considered a suitable approach for evaporative cooling and is not discussed in further detail below. We therefore suggest a system design that maximizes the evaporation at the cathode and incorporates a condenser only at the cathode exhaust.

### 3.4. Optimized fuel cell system operation

Based on the simulated stack performance and compressor power consumption, the maximum steady-state system power (at optimized pressure) can be calculated as a function of current density. Fig. 7a shows the impact of the operating temperature on the system power.

First, it can be seen, that there is no significant performance difference between the three main scenarios (80–95 °C) at low current densities ( $<0.8 \text{ A/cm}^2$ ). At higher loads, however, evaporative cooling performs better at higher operating temperature. The decrease in system performance at higher current densities is explained by two factors: first, the increase in the condenser pressure drop, which is more pronounced at lower operating temperatures (Fig. 6b), is limiting the minimal stack operating pressure and thus preventing to achieve the optimal system power. Second, the over-proportional increase in compressor power, which is also more prominent at lower operating temperature (Fig. 2a), exceeds the stack power and thus leads to the sharp drop in net system power. The course of system pressure and stoichiometry required to achieve the maximum net system power are presented in the supplementary information.

Since the exhaust gas condenser has been identified as the key component for evaporative cooling, the impact of its pressure drop is estimated by reducing the fitting factor  $\zeta$  by 25% (dashed lines in Fig. 7a). It can be seen, that a slight decrease in the fitting factor (i.e. a slight increase in condenser volume and mass) significantly effects the performance of the evaporatively cooled system at all operating temperatures. Note: The impact of the condenser outlet temperature on the pressure drop is neglected in the calculation of the optimized system power. Considering this effect would further decrease the performance at low operating temperature and only slightly affect the net system

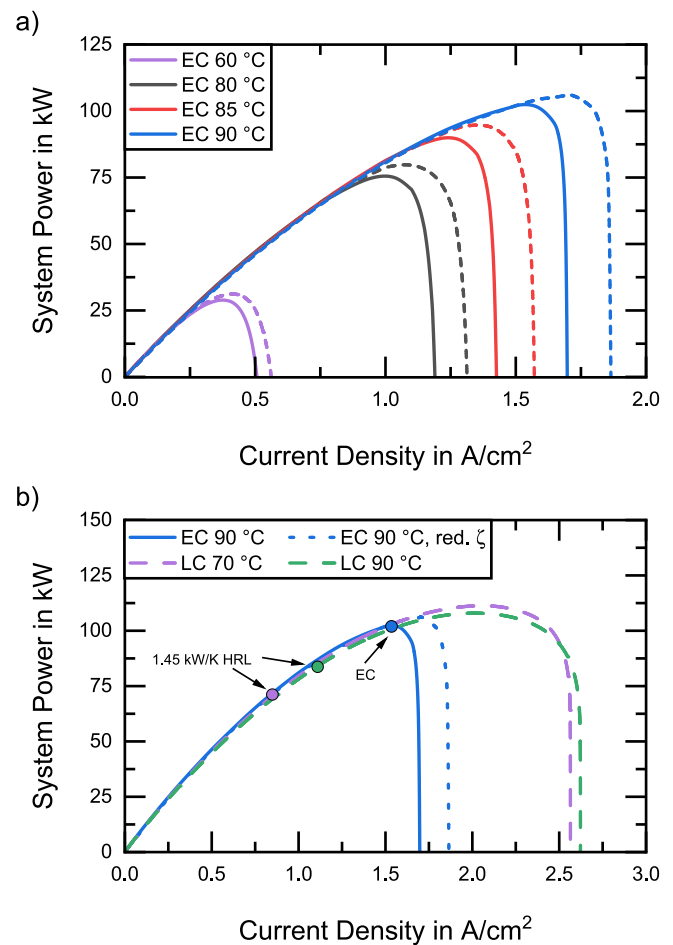
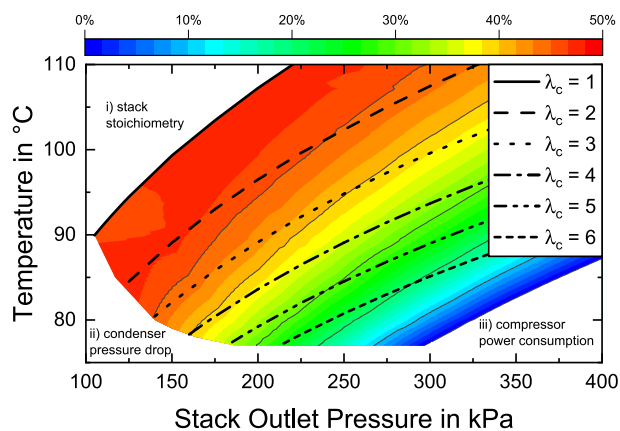


Fig. 7. a) optimized net system power as a function of current density for evaporative cooling at different operating temperatures and condenser pressure drop coefficients (dashed lines: reduction by 25%). b) comparison between evaporative cooling (solid and dotted, 25% reduced condenser pressure drop) and conventional cooling (dashed) at different operating temperatures. Markers indicate the respective limit with a 1.45 kW/K heat rejection limit (HRL) in FCEV.

power at higher operating temperatures and condenser outlet temperatures below 70 °C (see Fig. 6b).

The additional scenario at 60 °C (purple) provides insights into the behavior of evaporative cooling at low load points, such as at low-speed stop-and-go traffic, idling or low-speed cruising. Due to the lower waste heat, the operating temperature can be reduced as well. At 60 °C evaporative cooling works effectively up to a system power of 30 kW. Once the load point increases, the temperature will consequently rise and a new steady-state point is achieved. See Fig. 5 and the corresponding discussion in our previous work [45]. Furthermore, the limitations of evaporative cooling at low temperature operation and during freeze starts as well as corresponding mitigation strategies are discussed in our previous work [45].

When comparing evaporative cooling to the conventional cooling approach at two different temperatures (Fig. 7b), no significant performance deviation can be seen between the three approaches at lower current densities ( $<1.5 \text{ A/cm}^2$ ). At higher current densities, conventional cooling performs better at 70 °C than at 90 °C. Furthermore, conventional cooling shows a slightly higher peak power density than evaporative cooling. However, it has to be mentioned that conventional fuel cell systems are limited by the heat rejection capability of the vehicle to the environment. The blue and green markers in Fig. 7b indicate the DOE heat rejection limit of 1.45 kW/K for 70 °C and 90 °C respectively. This limits the continuous power output at around 70 kW



**Fig. 8.** Fuel cell system efficiency map, based on LHV at 1 A/cm<sup>2</sup> as a function of pressure, temperature and corresponding cathode stoichiometry to achieve thermal steady state.

at 70 °C and 85 kW at 90 °C at an ambient temperature of 25 °C. Evaporative cooling, however, is not directly limited by the convective heat rejection limit but the condensing radiator for water removal from the exhaust gas showing a similar behavior with temperature. However, due to the phase change, the condensation is more efficient which allows a closed water loop at 90 °C with the same volume requirements. This together with the absence of an external humidifier yields an increased power density at system level of up to 30%.

In order to determine the optimal operating parameter range for evaporative cooling, a system efficiency map, based on the lower heating value ( $\eta_{\text{sys}} = P_{\text{net}}/(\dot{n}_{\text{H}_2} \cdot \text{LHV})$ ), is calculated (see Fig. 8). It can be observed that the operating range is limited by (i) the stack performance at low pressure, high temperature and low stoichiometry (top left corner in Fig. 8), (ii) the pressure drop of the condenser, limiting the minimal stack outlet pressure (bottom left corner in Fig. 8) and (iii) the compressor power consumption at high pressure and high stoichiometry (bottom right corner in Fig. 8). Further, it can be seen, that the optimal efficiency is achieved at high temperature (80–90 °C), low pressure (125–150 kPa) and a corresponding cathode stoichiometry between 1.5 and 3.

#### 4. Conclusion

In this work, the interactions between the fuel cell stack and the BoP, when employing evaporative cooling, are analyzed using a zero-dimensional fuel cell system model. It is shown that evaporative cooling works very well and allows for a closed water loop over a broad range of operating conditions. The optimal system power output and highest efficiencies are achieved at high temperatures (80–90 °C), low pressure (125–150 kPa) and a corresponding stoichiometry between 1.5 and 3.

Scenarios with evaporative cooling at anode and cathode have been compared. It is shown that the compressor power increases over-proportionally with pressure for the cathode evaporative cooling concept whereas the hydrogen recirculation blower power increases with pressure in the anode evaporation concept. Pressure and stoichiometry have to be increased simultaneously in order to achieve a thermal steady state and ensure a constant operating temperature. Analyses of the condensation rates and the net system power have shown that the anode evaporation concept is not viable since the required condensation rates can only be achieved by compromising the system performance. Evaporation and condensation at the cathode, however allows for higher net system power as well as efficiency.

A comparison between evaporative cooling and conventional cooling has shown that there is no significant difference in performance at lower current densities. At higher current densities, evaporative cooling allows

for an additional gain of 20% in peak power (density) compared to conventional cooling.

The presented concept is feasible with state-of-the-art materials (e.g. PFSA membranes) at the lower end of the operating temperature requirements. However, a continuously increased operating temperature of 90 °C and beyond, that would further increase the peak system power and efficiency, would most probably require the development of more stable membranes. Additionally, it has to be investigated in future studies if evaporative cooling provides a sufficient humidification of the membrane at even more elevated temperatures without the need for external humidification.

The condenser has been identified as the one critical component for evaporative cooling on the system level. It is important to achieve a low outlet temperature, using materials suitable for deionized water and at the same time the pressure drop has to be minimized in order to allow a low system operating pressure for maximal system efficiency. Furthermore, volume mass and cost requirements have to be met. Future work has to focus on analyzing the trade-offs of the condensing radiator and estimate the volume and mass of a suitable component.

The optimal control of evaporatively cooled fuel cell systems requires a detailed knowledge of the interaction between operating conditions, cooling performance and net power output. Pressure and stoichiometry have to be controlled concurrently depending on the fuel cell load. The presented model can help to develop such control algorithms and due to low computational requirements, it could be implemented directly in fuel cell control units.

The results of this study underline the high potential of evaporative cooling to significantly reduce fuel cell system volume, mass (up to 30%) and cost.

#### CRediT authorship contribution statement

**Michael Striednig:** Methodology, Formal analysis, Software, Visualization, Investigation, Writing – original draft. **Thomas J. Schmidt:** Resources, Project administration, Writing – review & editing. **Felix N. Büchi:** Funding acquisition, Conceptualization, Writing – review & editing, Supervision.

#### Declaration of competing interest

The authors declare that they have no known competing financial interests or personal relationships that could have appeared to influence the work reported in this paper.

#### Acknowledgements

The authors gratefully acknowledge Innosuisse for funding through the Swiss Competence Center for Energy Research: Efficient Technologies and Systems for Mobility (SCCER Mobility). Further, the authors would like to thank Magali Cochet, Pierre Boillat, Adrian Mularczyk, Salvatore de Angelis, Mayank Sabharwal, Andreas Michalski and Jens Eller (PSI), as well as Robert Herrendörfer, Roman Vetter and Jürgen Schumacher (ZHAW) for many fruitful discussions on evaporative cooling modelling.

#### Appendix A. Supplementary data

Supplementary data to this article can be found online at <https://doi.org/10.1016/j.jpowsour.2022.231720>.

#### References

- [1] T. Yoshida, K. Kojima, Toyota MIRAI fuel cell vehicle and progress toward a future hydrogen society, *Electrochem. Soc. Interf.* 24 (2015) 45, <https://doi.org/10.1149/2.F03152if>.

- [2] W. Sung, Y.-I. Song, K.-H. Yu, T.-W. Lim, Recent advances in the development of Hyundai Kia's fuel cell electric vehicles, *SAE Int. J. Engines*. 3 (2010) 768–772, <https://doi.org/10.4271/2010-01-1089>.
- [3] M. Matsunaga, K. Kimura, T. Fukushima, T. Ogawa, K. Ojima, Fuel cell powertrain for FCX clarity, *Honda RD Tech. Rev.* 21 (2009) 9.
- [4] E. Bauer, et al., Path to Hydrogen Competitiveness: A Cost Perspective - Hydrogen Council. <https://hydrogencouncil.com/en/path-to-hydrogen-competitiveness-a-cost-perspective/>. (Accessed 21 March 2020).
- [5] Hyundai delivers first XCIENT Fuel Cell trucks to Switzerland, *Fuel Cell. Bull.* 3 (2020), [https://doi.org/10.1016/S1464-2859\(20\)30328-X](https://doi.org/10.1016/S1464-2859(20)30328-X), 2020.
- [6] J. Juriga, Hyundai Motor Group's Development of the Fuel Cell Electric Vehicle, 2020. [https://www.hydrogen.energy.gov/pdfs/htac\\_may2012\\_hyundai.pdf](https://www.hydrogen.energy.gov/pdfs/htac_may2012_hyundai.pdf).
- [7] Y. Naganuma, K. Manabe, H. Imanishi, Y. Nonobe, Development of system control for rapid warm-up operation of fuel cell, *SAE Int. J. Altern. Powertrains*. 1 (2012) 365–373, <https://doi.org/10.4271/2012-01-1230>.
- [8] M. Striednig, S. Brandstätter, M. Sartory, M. Klell, Thermodynamic real gas analysis of a tank filling process, *Int. J. Hydrogen Energy* 39 (2014) 8495–8509, <https://doi.org/10.1016/j.ijhydene.2014.03.028>.
- [9] B.G. Pollet, I. Staffell, J.L. Shang, Current status of hybrid, battery and fuel cell electric vehicles: from electrochemistry to market prospects, *Electrochim. Acta* 84 (2012) 235–249, <https://doi.org/10.1016/j.electacta.2012.03.172>.
- [10] V. Das, S. Padmanaban, K. Venkitesh, R. Selvamuthukumar, F. Blaabjerg, P. Siano, Recent advances and challenges of fuel cell based power system architectures and control – a review, *Renew. Sustain. Energy Rev.* 73 (2017) 10–18, <https://doi.org/10.1016/j.rser.2017.01.148>.
- [11] A. Wilson, G. Kleen, D. Papageorgopoulos, *Fuel Cell System Cost - 2017, DOE Hydrogen and Fuel Cells Program Record*, 2017.
- [12] U.S. Department of Energy, Fuel Cell Technologies Office Multi-Year Research, Development, and Demonstration Plan, 2016. [https://www.energy.gov/sites/default/files/2017/05/f34/fcto\\_myrdid\\_fuel\\_cells.pdf](https://www.energy.gov/sites/default/files/2017/05/f34/fcto_myrdid_fuel_cells.pdf).
- [13] G. Zhang, S.G. Kandlikar, A critical review of cooling techniques in proton exchange membrane fuel cell stacks, *Int. J. Hydrogen Energy* 37 (2012) 2412–2429, <https://doi.org/10.1016/j.ijhydene.2011.11.010>.
- [14] A. De las Heras, F.J. Vivas, F. Segura, J.M. Andújar, From the cell to the stack. A chronological walk through the techniques to manufacture the PEMFCs core, *Renew. Sustain. Energy Rev.* 96 (2018) 29–45, <https://doi.org/10.1016/j.rser.2018.07.036>.
- [15] A. Kusoglu, A.Z. Weber, New insights into perfluorinated sulfonic-acid ionomers, *Chem. Rev.* 117 (2017) 987–1104, <https://doi.org/10.1021/acs.chemrev.6b00159>.
- [16] E.J. Choi, S.H. Hwang, J. Park, M.S. Kim, Parametric analysis of simultaneous humidification and cooling for PEMFCs using direct water injection method, *Int. J. Hydrogen Energy* 42 (2017) 12531–12542, <https://doi.org/10.1016/j.ijhydene.2017.03.201>.
- [17] S.H. Hwang, M.S. Kim, An experimental study on the cathode humidification and evaporative cooling of polymer electrolyte membrane fuel cells using direct water injection method at high current densities, *Appl. Therm. Eng.* 99 (2016) 635–644, <https://doi.org/10.1016/j.applthermaleng.2016.01.091>.
- [18] D.L. Wood, J.S. Yi, T.V. Nguyen, Effect of direct liquid water injection and interdigitated flow field on the performance of proton exchange membrane fuel cells, *Electrochim. Acta* 43 (1998) 3795–3809, [https://doi.org/10.1016/S0013-4686\(98\)00139-X](https://doi.org/10.1016/S0013-4686(98)00139-X).
- [19] R. Cohen, Fuel Cell Evaporative Cooling Using Fuel as a Carrier Gas, 1991. US4994331A.
- [20] H.R. Kunz, Solid Polymer Electrolyte Fuel Cell System with Porous Plate Evaporative Cooling, 1992. CA1309127C.
- [21] A. Warburton, D. Mossop, B. Burslem, P. Rama, P. Adcock, J. Cole, J. Edwards, D. Ninan, M. Provost, Development of an Evaporatively Cooled Hydrogen Fuel Cell System and its Vehicle Application, 2013, <https://doi.org/10.4271/2013-01-0475>, 2013-01–0475.
- [22] C.J. Carnevale, T.W.P. Jr, R.M. Darling, P. Badrinarayanan, M.L. Perry, Hybrid Bipolar Plate for Evaporatively Cooled Fuel Cells, US9570763B2, 2017.
- [23] M.L. Perry, J.P. Meyers, R.M. Darling, C. Evans, R. Balliet, Evaporatively-cooled PEM fuel-cell stack and system, *ECS Trans.* 3 (2006) 1207, <https://doi.org/10.1149/1.2356240>.
- [24] T. Scheibert, Verdampfungsgekühltes Brennstoffzellensystem und Verfahren zum Betreiben eines verdampfungsgekühlten Brennstoffzellensystems, EP2225789B1, 2011.
- [25] M. Katz, Fuel Cell Evaporative Cooler, 1993, US5206094A.
- [26] S.G. Goebel, Evaporative Cooled Fuel Cell, US6960404B2, 2005.
- [27] V. Maisotsenko, L.E. Gillan, T.L. Heaton, A.D. Gillan, Fuel Cell Systems with Evaporative Cooling and Methods for Humidifying and Adjusting the Temperature of the Reactant Streams, US6779351B2, 2004.
- [28] J. Stedman, Fuel Cell with Evaporative Cooling, US3761316A, 1973.
- [29] M. Cochet, A. Forner-Cuenca, V. Manzi, M. Siegwart, D. Scheuble, P. Boillat, Novel concept for evaporative cooling of fuel cells: an experimental study based on neutron imaging, *Fuel Cell.* 18 (2018) 619–626, <https://doi.org/10.1002/fuce.201700232>.
- [30] A. Forner-Cuenca, J. Biesdorf, L. Gubler, P.M. Kristiansen, T.J. Schmidt, P. Boillat, Engineered water highways in fuel cells: radiation grafting of gas diffusion layers, *Adv. Mater.* 27 (2015) 6317–6322, <https://doi.org/10.1002/adma.201503557>.
- [31] J. Dujc, A. Forner-Cuenca, P. Marmet, M. Cochet, R. Vetter, J.O. Schumacher, P. Boillat, Modeling the effects of using gas diffusion layers with patterned wettability for advanced water management in proton exchange membrane fuel cells, *J. Electrochem. Energy Convers. Storage*. 15 (2018), 021001, <https://doi.org/10.1115/1.4038626>. –021001.
- [32] M.A. Safi, J. Mantzaras, N.I. Prasianakis, A. Lamibrac, F.N. Büchi, A pore-level direct numerical investigation of water evaporation characteristics under air and hydrogen in the gas diffusion layers of polymer electrolyte fuel cells, *Int. J. Heat Mass Tran.* 129 (2019) 1250–1262, <https://doi.org/10.1016/j.ijheatmasstransfer.2018.10.042>.
- [33] M.A. Safi, N.I. Prasianakis, J. Mantzaras, A. Lamibrac, F.N. Büchi, Experimental and pore-level numerical investigation of water evaporation in gas diffusion layers of polymer electrolyte fuel cells, *Int. J. Heat Mass Tran.* 115 (2017) 238–249, <https://doi.org/10.1016/j.ijheatmasstransfer.2017.07.050>.
- [34] L. Capone, P. Marmet, L. Holzer, J. Dujc, J.O. Schumacher, A. Lamibrac, F.N. Büchi, J. Becker, An ensemble Monte Carlo simulation study of water distribution in porous gas diffusion layers for proton exchange membrane fuel cells, *J. Electrochem. Energy Convers. Storage* 15 (2018), <https://doi.org/10.1115/1.4038627>, 031005–031005–10.
- [35] S. Lal, A. Lamibrac, J. Eller, F.N. Büchi, Determination of water evaporation rates in gas diffusion layers of fuel cells, *J. Electrochem. Soc.* 165 (2018) F652–F661, <https://doi.org/10.1149/2.0831809jes>.
- [36] I.V. Zenyuk, A. Lamibrac, J. Eller, D.Y. Parkinson, F. Marone, F.N. Büchi, A. Z. Weber, Investigating evaporation in gas diffusion layers for fuel cells with X-ray computed tomography, *J. Phys. Chem. C* 120 (2016) 28701–28711, <https://doi.org/10.1021/acs.jpcc.6b10658>.
- [37] A. Mularczyk, A. Michalski, M. Striednig, R. Herrendörfer, T.J. Schmidt, F.N. Büchi, J. Eller, Mass Transport limitations of water evaporation in polymer electrolyte fuel cell gas diffusion layers, *Energies* 14 (2021) 2967, <https://doi.org/10.3390/en14102967>.
- [38] P.-Y.A. Chuang, M.A. Rahman, F. Mojica, D.S. Hussey, D.L. Jacobson, J. M. LaManna, The interactive effect of heat and mass transport on water condensation in the gas diffusion layer of a proton exchange membrane fuel cell, *J. Power Sources* 480 (2020), 229121, <https://doi.org/10.1016/j.jpowsour.2020.229121>.
- [39] M. Sarker, M.A. Rahman, F. Mojica, S. Mehrzi, W.J.M. Kort-Kamp, P.-Y. A. Chuang, Experimental and computational study of the microporous layer and hydrophobic treatment in the gas diffusion layer of a proton exchange membrane fuel cell, *J. Power Sources* 509 (2021), 230350, <https://doi.org/10.1016/j.jpowsour.2021.230350>.
- [40] M. Cochet, A. Forner-Cuenca, V. Manzi-Orezzoli, M. Siegwart, D. Scheuble, P. Boillat, Enabling high power density fuel cells by evaporative cooling with advanced porous media, *J. Electrochem. Soc.* 167 (2020), 084518, <https://doi.org/10.1149/1945-7111/ab8e82>.
- [41] M. Schultze, J. Horn, A control oriented simulation model of an evaporatively cooled polymer electrolyte membrane fuel cell system, *IFAC Proc.* 44 (2011) 14790–14795, <https://doi.org/10.3182/20110828-6-IT-1002.00311>.
- [42] A. Fly, R.H. Thring, System thermal and water balance in an evaporatively cooled PEM fuel cell vehicle, in: *Veh. Therm. Manag. Syst. Conf. Proc. VTMS11*, Woodhead Publishing, 2013, pp. 267–277, <https://doi.org/10.1533/9780857094735.6.267>.
- [43] A. Fly, R.H. Thring, Temperature regulation in an evaporatively cooled proton exchange membrane fuel cell stack, *Int. J. Hydrogen Energy* 40 (2015) 11976–11982, <https://doi.org/10.1016/j.ijhydene.2015.04.086>.
- [44] A. Fly, R.H. Thring, A comparison of evaporative and liquid cooling methods for fuel cell vehicles, *Int. J. Hydrogen Energy* 41 (2016) 14217–14229, <https://doi.org/10.1016/j.ijhydene.2016.06.089>.
- [45] M. Striednig, M. Cochet, P. Boillat, T.J. Schmidt, F.N. Büchi, A model based investigation of evaporative cooling for polymer electrolyte fuel cells – stack level analysis, *J. Power Sources* 517 (2022), 230706, <https://doi.org/10.1016/j.jpowsour.2021.230706>.
- [46] S. Brandstätter, M. Striednig, D. Aldrian, A. Trattner, M. Klell, T. Dehne, C. Kügele, M. Paulweber, Highly Integrated Fuel Cell Analysis Infrastructure for Advanced Research Topics, 2017, <https://doi.org/10.4271/2017-01-1180>, 2017-01–1180.
- [47] J. Kancsár, M. Striednig, D. Aldrian, A. Trattner, M. Klell, C. Kügele, S. Jakubek, A novel approach for dynamic gas conditioning for PEMFC stack testing, *Int. J. Hydrogen Energy* 42 (2017) 28898–28909, <https://doi.org/10.1016/j.ijhydene.2017.09.076>.
- [48] The MathWorks Inc., MATLAB® Documentation, 2021 accessed, <http://www.mathworks.de/de/help/matlab/>. (Accessed 16 April 2021).
- [49] J.R. Dormand, P.J. Prince, A family of embedded Runge-Kutta formulae, *J. Comput. Appl. Math.* 6 (1980) 19–26, [https://doi.org/10.1016/0771-050X\(80\)90013-3](https://doi.org/10.1016/0771-050X(80)90013-3).
- [50] W. Gu, D.R. Baker, Y. Liu, H.A. Gasteiger, Proton exchange membrane fuel cell (PEMFC) down-the-channel performance model, in: *Handb. Fuel Cells*, John Wiley & Sons, Ltd, 2003, <https://doi.org/10.1002/9780470974001.f500044>.
- [51] S.A. Klein, G. Nellis, *Thermodynamics*, Cambridge University Press, New York, 2012.
- [52] E.W. Lemmon, I.H. Bell, M.L. Huber, M.O. McLinden, NIST Standard Reference Database 23: Reference Fluid Thermodynamic and Transport Properties-REFPROP, Version 10.0, National Institute of Standards and Technology, 2018, <https://doi.org/10.18434/T4/1502528>.